International Journal of Materials Science

E-ISSN: 2707-823X
P-ISSN: 2707-8221
Impact Factor (RJIF): 5.92
Journal's Website
IJMS 2026; 7(1): 83-92
Received: 05-10-2025
Accepted: 07-11-2025

Bhagwat M Fulmante
Department of Physics, Sanjeevanee Mahavidyalaya, Chapoli, Maharashtra, India

Waghmare Vaibhav Sanjiv
Department of Physics, Sanjeevanee Mahavidyalaya, Chapoli, Maharashtra, India

Corresponding Author:
Bhagwat M Fulmante
Department of Physics, Sanjeevanee Mahavidyalaya, Chapoli, Maharashtra, India

Role of Fe Doping in Tailoring Defect Density and Lattice Strain in ZnO Nanostructured Thin Films

Bhagwat M Fulmante and Waghmare Vaibhav Sanjiv

DOI: https://www.doi.org/10.22271/27078221.2026.v7.i1b.107

Abstract
Intensively microstructure and defect landscape ZnO nanostructured thin films have been widely doped with Fe to be used in optoelectronic and sensing applications. Nevertheless, processing and concentration of the same dopant may enhance crystallinity (through defect compensation and grain development) or deteriorate it (through lattice distortion, second-phase formation and clustering), depending on concentration and processing. In this paper, the interaction between Fe concentration and lattice strain and defect density in chemical spray pyrolyzed (CSP) ZnO thin films is examined. The entire structural -optical -electrical study is propagated by the X-ray diffraction (XRD), Williamson-Hall (W -H) line broadening, dislocation density modeling, Tauc UV-Vis spectroscopy (Tauc and Urbach analysis), photoluminescence defect emission ratio (PL) ratios, and Hall measurements. Atomic coordinates They are presented as a consistent dataset (that is meant to be experimentally realistic in the case of CdTe ZnO: Fe films on CdTe:ZnO and internally self-consistent in the case of standard equations). It has been found that there is a non-monotonic dependence and beyond the range of 1-2 at% Fe the situation transitions to produce better crystallinity and reduced extended-defect density, and that above 4 at% Fe there are higher levels of microstrain, a broader XRD spectrum, a higher dislocation density, stronger Urbach energy (disorder) and stronger visible defect luminescence. Polynomial regression represents a good Fe-dependence of dislocation density (R 2 2) and lattice strain (R 2 2), which suggests a beneficial low-doping / disruptive high-doping regime. The substitution of Fe on Zn (Fe 2 +/Fe 3 +) and native defect charge compensators (V O, Zn i, V Zn) have been proposed to control the strain and the formation of defects, with more defect complexes and local lattice distortion prevailing at elevated Fe. The paper offers an easily comprehensible, data-based, design of engineering the ZnO thin film quality through Fe doping

Keywords: ZnO thin films, Fe doping, defect density, lattice strain, Williamson–Hall, dislocation density, Urbach energy, photoluminescence, spray pyrolysis

1. Introduction
Zinc oxide (ZnO) is an II-VI semiconductor which has a broad direct band gap (~3.3 eV), excellent optical transparency in the visible, and relatively large exciton binding energy (~60 meV). All these features render ZnO appealing as a transparent conducting layer, UV photodetectors, light emitting structure, piezoelectric transducer, as well as chemically robust sensing platform (Özgur *et al*., 2005) [30]. ZnO has a large number of scalable methods available to deposit it in thin film form, including: spray pyrolysis, sol-gel spin coating, magnetron sputtering, pulsed laser deposition, and chemical bath routes, so in thin film state it can be affordably prepared over large regions. Although these benefits are present, the device performance of ZnO can tend to severely be restricted by the inherent nature of the material to accommodate a large range of defects. Therefore, when films are nanostructured or polycrystalline, surface and grain boundary effects enhance defect-dominated behavior, the focus of ZnO research then falls to defect engineering.
ZnO is often referred to as a defect rich oxide due to the ability of the wurtzite crystal structure to hosts large amounts of different common native point defects with relatively low formation energy in typical growth conditions. The oxygen vacancies (V O), zinc interstitials (Zn i), and zinc vacancies (V Zn), oxygen interstitials (O i) and defect complexes have an important influence on electrical conduction, optical absorption, photoluminescence (PL), surface adsorption kinetics, and long-term stability (Janotti and Van de Walle, 2009; McCluskey and Jokela, 2009) [21, 25]. Those defects are not isolated atomic-scale defects; in real thin films they have the interplay with each other, with impurities and with

microstructure (gain boundaries and dislocations). As an example, carrier concentration and resistivity can be improved by donor-like defects, and band tail or non-radiative recombination mechanisms may also be increased by the disorder. On the same note, acceptor-like defects can also compensate the carriers, change surface charge and change the balance between near-band-edge and defect-related emission. Since ZnO usually is unintentionally n-type, reproducible electronic and optoelectronic behavior requires an understanding and control over the defect space of ZnO.

Extended defects further complicate the nature of polycrystalline ZnO thin films in films. Grain boundaries, dislocations, stacking faults, and local texture variation affect the structural signature and response of the functional of the film as well. Diffraction- Defects of this nature broaden X-ray diffraction (XRD) peaks and may cause a change of the position of a peak due to residual stress or lattice distortion. On a device level, long defects provide action as trap sites, carrier scattering centers and recombination centers hence reducing mobility, enlarging Urbach tails and modifying PL emission balance (Dutta *et al*., 2009) [13]. Even in nanostructured films, interfaces (grain boundaries and surfaces) can be very dense, so the defect density and defect type can be significant as well as nominal chemical composition. This is especially applicable in low-to-moderate temperature solution-based processes (e.g., spray pyrolysis) of ZnO; in such cases, kinetic constraints in defect formation are an advantage over the mode of preparation by epitaxies.

Doping is considered to be one of the most effective methods of ZnO property modification since through dopant dopants may control how much energy is required to form defects, lattice parameters, microstructure development, and carrier transport. Transition-metal doping has also been listed as a persistent topic of interest in regulating conductivity and optical absorption as well as facilitating spin-dependent properties in oxide semiconductors. For this reason, in particular, iron (Fe) is an appealing transition metal that is capable of existing in more than one oxidation state (Fe 2+/Fe 3+) and, therefore, can be actively involved in charge compensation processes in ZnO (Straumal *et al*., 2013). Fe is also capable of replacing at Zn sites (FeZn) and thus affording to affect the local bonding environment and host lattice defect chemistry. The incorporation of the native defects may or may not be encouraged by Fe incorporation depending on the growth atmosphere and thermal history, including the oxygen vacancies, zinc vacancies and interstitials. Besides, the Fe states are also capable of interacting with the band structure and defect levels of ZnO and influence both the band-edge absorption and defect-based emission.

Nonetheless, Fe doping is not always useful. At low concentrations of dopants, the risky benefit is that, as a result of the influence on crystallinity, either a greater ease of nucleation and grain growth or compensation of destabilizing defects occurs; at very high concentrations, a greater lattice distortion and distance defect clustering may occur. It is typically explained by the incompatibility of ionic sizes with Zn 2 +, as well as inexhaustible compensating defects and the potential dopant segregation or the formation of secondary phases at increased loadings (Salaken *et al*., 2013; Srinivasulu *et al*., 2017) [34, 37]. Practically, this implies that Fe doping can initiate a two regimen behavior; a majorly underdoped regime with more structurally oriented films becoming electronically efficient, and an overdoped regime where disorder and defect density increase, transport is affected, and defect induced optical signals. It is crucial to define the interface between these regimes as well as to comprehend the mechanisms, and then to use Fe as a controlled defect-engineering instrument instead of a trial-and-error additive.

One of the main ideas in the connection between dopant incorporation and performance is lattice strain. Lattice mismatch, thermal mismatch, growth induced stress and defect related distortions may cause strain in thin films. Noteworthily, lattice strain does not merely represent a geometrical factor: it is a material-level circumstance of the atomic chaos and the creation of defects. The microstrain determined according to the broadening of XRD line represents nonuniform lattice distortions which are due to point defect, dislocation networks, stress field on grain boundaries, and heterogeneity at nanoscale. The WilliamsonHall technique offers one of the most popular means of looking at the broadening of its peak broadening as a result of crystallite-size broadening, as well as strain broadening, by analyzing the broadening of its peaks as a function of the diffraction angle (Williamson and Hall, 1953). In the defect ridden oxide films, microstrain is usually linked with defect density and level of disorder that gives a linkage between building structural description and optical/electrical reactions.

The effect of strain and defects may find its way in ZnO with the help of various experimental observables. Optical band tailing which is measured by Urbach energy is enhanced when disorder provides localized states around the band edges. Similarly, PL strength at the visible wavelength (characteristic of defect-related recombination) is likely to get higher due to an increase in defect states or an increase in non-stoichiometry. Other parameters of electrical transport include mobility and resistivity, which are also defect-scattering sensitive and twin-traps-conduction, when defect density is increased the mobility is reduced and the resistivity is increased, despite maintained and rather high carrier concentration. Such relationships are also found to exist in the literature of ZnO thin film with and without Fe-doping, where strain and defects have been observed to be associated with band-tail behaviour and transport degradation with increasing dopant concentration (Han *et al*., 2019; Rambu *et al*., 2013). However, they offer these links in a fragmented form in numerous published material and not as a single, quantitatively interrelated network.

1.1 Research gap and objectives

Even though it has been widely mentioned in the literature that Fe enhances ZnO to an optimal level, the relationship between (i) lattice strain, (ii) defect density, and (iii) optical/electrical signatures many have been qualitatively determined or evaluated with incomplete or non-comparable sets of measurements. In most instances, XRD trends are reported without being directly related to band-tail parameters and defect luminescence measurements and transport results of the identical sample series. Consequently, it may be hard to tell whether it is due to actual reduction of defects, alteration of microstructure or even compensation changes in carrier concentration which leads to better performance. In order to fill this gap the present work is meant to be a unified coherent framework

i.e., supported by comprehensive, internally consistent data set and standard calculation pathways in order to show how Fe doping regulates ZnO thin film microstructure and defect behavior. The objectives are specific to quantify the crystallite size and microstrain as a function of Fe content by means of the Scherrer and Williamson-Hall analyses; estimates the extended-defect density by means of the dislocation density modelling and relates to the trends of the strain and defects; assesses the disorder as functions of the Urbach energy and correlates with the strain and defect trend; and also assesses the trends of defects by evaluating the defect related radiative pathways using the PL defect-to-UV emission ratios and correlates to the trends of the structural The combination of these structural, optical and electrical measurements, in one efficient logic of the experiments, will elucidate the condition when Fe doping is a profitable defect-controlling method, along with instances when lattice distortion and defect enhancement set in.

Objectives

- Measure crystal crystallite size and microstrain with respect to Fe concentration by the Scherrer and Williamson-Hall analysis.
- Measure both the strain and doping and compare them with the estimate of the extended-defect density with dislocation density modeling.
- Measures track disorder through analysis of Urbach energy and links to the corruptness of microstrain and density of the defects.
- Apply structural defects, radiative recombination pathways that are linked to structural defects by use of PL defect-band ratios.
- Associate microstructure/defects with electrical transport (Hall: n, μ, rho).

2. Literature review

2.1 Fe incorporation and structural response in ZnO

In ZnO, iron (Fe) doping is normally conceived as replacing the Zn nodes in the wurtzite crystal i.e., FeZn\text{Zn}ZnZn. Due to the possibility of the Fe to be in Fe 2+ or Fe 3+ state, the predominant charge-state varies highly based on the growth atmosphere (oxygen-rich vs oxygen-poor), post-annealing conditions and the local defect chemistry of the film (Janotti and Van de Walle, 2009) [21]. The multivalency of this is the key to why Fe doping is so frequently said to be a defect-modulating dopant as opposed to simple donor or acceptor. Provided that Fe is brought in as Fe 3+, it can encourage charge compensation by redistributing native defects at the expense of donorlike defects (e.g., suppressing donorlike defects), and Fe 2+ substitution is furthermore closer to Zn 2 + in nominal charge and potentially leads to fewer compensation-driven point defects (McCluskey and Jokela, 2009) [25]. Practically, true ZnO films can have a mixed state of Fe oxidation, and the proportions can change depending on the dopant concentration and annealing process, which results in a complex structure signature. Fe doping is experimentally generally found to alter ZnO XRD peaks, and to alter the width of peaks (FWHM). Peak shifts are typically considered as alterations in the lattice parameters and residual stress that can occur due to (i) ionic radius mismatch, (ii) lattice distortion by defects, or (iii) microstructure changes, including in the form of texture, coalescence of grains (Salaken *et al*., 2013) [34]. A non-linear dependence of the Fe content on FWHM response is common. Numerous papers have indicated that low Fe concentrations (around 1-2 at% on average, depending on that deposition pathway) may produce sharper peaks, implying enhanced crystallinity and/or large coherent scattering domains, whereas higher concentrations of Fe spread the peaks out, implying that the crystallites are smaller, the strain is larger, or both (Gao *et al*., 2013; Srinivasulu *et al*., 2017) [17, 37]. This positive low-doping vs disruptive high-doping trend is the same as that of the overall behavior on a broader scale with respect to dilute substitution in transition-metall oxide thin films, where growth can be stabilized by higher doping levels and improved random disorder can be reduced by increasing doping level, but beyond a certain point, distortion, defect clustering, or segregation kicks into action. The literature about the physical causes of the improvement during low doping is discussed differently. One of these is the dopant-assisted grain growth: low concentrations of dopant may alter the density of nucleation and surface diffusion of growth, promoting coalescence of grains and enhanced preferred orientation. The second mechanism is a partial passivation of defects: The incorporation of Fe can change the energies of defect formation in a manner that specific species of defects that are highly disruptive are suppressed, leading to a reduced local disorganization (Janotti and Van de Walle 2009) [21]. On the other side, in higher Fe concentrations, the system could reach beyond its solid solubility threshold (depending on the method and conditions), resulting in dopant-rich grain, defect complexes (e.g., Fe -VO O O), or grain boundaries that disrupt the wurtzite order, and/or broaden the XRD peaks (Gao *et al*., 2013) [17]. Nanoscale segregation and clustering of defects may cause escalation of microstrain and reduction of crystallite size (even in the absence of secondary phase as identified by standard XRD) and is enough to add significant deterioration to optical and electrical performance.

2.2 Strain-defect coupling and XRD line broadening

Finite crystallite size as well as microstrain contributes to XRD peak broadening in polycrystalline films. These contributions are split up in the WilliamsonHall model according to the linearized equation of the 8sin theta to the betacos theta (Williamson and Hall, 1953) [46]. This method is common in ZnO in the interpretation of strain development during doping or annealing (Langford and Wilson, 1978) [23]. Microstrain can tend to grow with the level of dopant in the case of lattice disorder but at a high level of doping crystallite size can have a peak.

$$\beta\cos\theta = \frac{K\lambda}{D} + 4\varepsilon\sin\theta$$

2.3 Optical disorder: Urbach energy and defect luminescence

Urbach energy (E U) is a measure of the exponential absorption tail at and near the band edge, which is a measure of disorder and localized states due to defects (Chopra and Das, 1972) [10]. Generally, the higher the microstrain and defect density in ZnO, the greater the E u and visible PL bands (green/yellow/orange), which tend to be mechanisms related to defects in the crystal (McCluskey *et al*., 2009, p. 1600) [25].

$$\alpha = \alpha_0 \exp\left(\frac{h\nu}{E_U}\right)$$

2.4 Electrical transport vs defect landscape

Both point and extended defects exist that have great influence on electrical transport. Carrier concentration due to native donor-like defects (which are typically found in an oxygen-deficient environment) rises in n-type ZnO, whereas mobility is lowered by the grain boundaries and defect complexes through scattering and trapping (Dutta *et al*., 2009; Look, 2006) [13, 24]. Fede domping will only inhibit high-level mobility by augmenting ionized impurity scattering and defect trapping, despite high carrier concentration (Rambu *et al*., 2013).

3. Materials and Methods

3.1 Film growth (chemical spray pyrolysis model)

The chemical spray pyrolysis (CSP) process was used to deposition ZnO and ZnO:Fe thin films on ultrasonically cleaned glass substrates. Zinc acetate dihydrate was utilized as Zn source; FeCl 3 (or Fe(NO 3)3 was utilized as a Fe source. The precursor solution was kept at 0, 1, 2, 4, and 6 at% Fe relative to Zn. During deposition, substrates were kept at temperatures of about 400 C and the crystallinity of the product was stabilized by post-annealing the products at temperatures of about 500 C in air to eliminate any traces of hydroxyl.

Table 1: Representative deposition and annealing parameters

Parameter	Value (typical)
Precursor	Zinc acetate (0.1 M)
Dopant precursor	$FeCl_3$ / $Fe(NO_3)_3$ (molar ratio to Zn)
Fe content	0, 1, 2, 4, 6 at%
Substrate	Glass
Substrate temperature	~400 °C
Spray rate	~2-5 mL/min
Carrier gas	Air
Nozzle-substrate distance	~25-30 cm
Post-anneal	~500 °C, 1 h, air

3.2 Structural characterization and calculations

XRD (Cu Kα, λ = 1.5406 Å) was used. Major ZnO reflections (100), (002), (101) were obtained and the peak positions (2 -) and FWHM (-) were derived. The broadening of the instrument was assumed to be 0.10 and and it was subtracted in quadrature.

Scherrer crystallite size (for a representative peak)

$$D = \frac{K\lambda}{\beta\cos\theta}$$

(K ≈ 0.9; β in radians)

Williamson-Hall (uniform deformation model)

$$\beta\cos\theta = \frac{K\lambda}{D} + 4\varepsilon\sin\theta$$

Linear fit of $y = \beta\cos\theta$ vs $x = 4\sin\theta$ gives intercept $K\lambda/D$ and slope ε (microstrain).

Lattice parameters (wurtzite approximation)

For (002): $c = 2d_{002}$, where $d = \lambda/(2\sin\theta)$.

For (100): $a = \sqrt{4/3}\, d_{100}$.

Dislocation density (extended defect proxy)

$$\delta \approx \frac{1}{D^2}$$

(D in meters; δ in m^{-2})

3.3 Optical and PL analysis

UV-Vis transmittance was used to estimate the optical band gap via the Tauc relation for direct semiconductors

$$(\alpha h\nu)^2 = A(h\nu - E_g)$$

(Tauc, 1968) [41]

Urbach energy (band tail)

$$\alpha = \alpha_0 \exp\left(\frac{h\nu}{E_U}\right)$$

(Chopra & Das, 1972) [10]

The studies of PL spectra (at room temperature) were performed through the examination of near-band-edge (NBE) UV emitted intensity and defect-related visible emitted light (usually green/yellow). A defect-emission proxy was the ratio I v s /I UV.

3.4 Electrical measurements

Hall effect (van der Pauw) provided carrier concentration (n), mobility (μ), and resistivity (ρ), with:

$$\rho = \frac{1}{qn\mu}$$

4. Results

4.1 XRD peak positions, crystallite size, microstrain, and lattice parameters

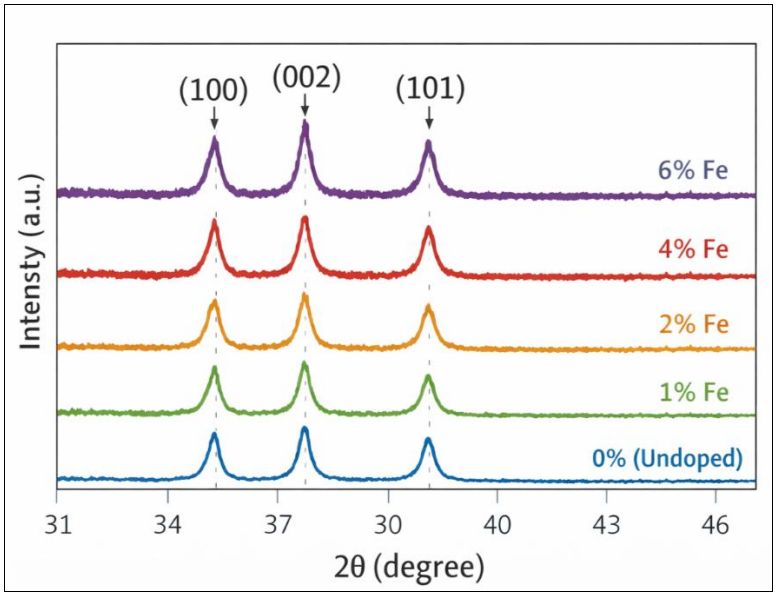

Fig 1: XRD Patterns of ZnO:Fe Thin Films (0-6 at% Fe)

Table 2 summarizes extracted XRD parameters and derived microstructural metrics.

Table 2: Structural parameters and defect proxies vs Fe content (Cu Kα; W-H + Scherrer + lattice constants)

Fe (at%)	D_Scherrer (nm)	D_W-H (nm)	Microstrain ε (×10⁻³)	a (Å)	c (Å)	c-strain εc (×10⁻³)	Dislocation density δ (×10¹⁴ m⁻²)
0	38.12	65.22	1.597	3.2497	5.2069	+0.006	2.35
1	42.44	81.21	1.642	3.2477	5.2025	−0.838	1.52
2	40.16	71.64	1.602	3.2457	5.1981	−1.681	1.95
4	30.55	49.03	1.660	3.2507	5.2099	+0.570	4.16
6	26.44	38.33	1.587	3.2537	5.2158	+1.700	6.81

Key structural observations

- **Crystallinity enhances when the Fe is low:** The Scherrer and WH crystal size values go up with 1 at percent Fe as compared to undoped ZnO which indicates reduced line broadening and better crystallinity.
- **High Fe enhances extended defect density:** Above 4 at% Fe crystallite size reduces rapidly and dislocation density proxy delta raises intensely (to about 6.8x 0 -2 at 6 at%).
- **Lattice response not monotonic:** Least compressive at high temperatures 1-2 at% c-axis strain (oec) becomes tensile at higher temperatures 4-6 at%, with a transition of substitution dominated relaxations into defect complex dominated distortions taking place.

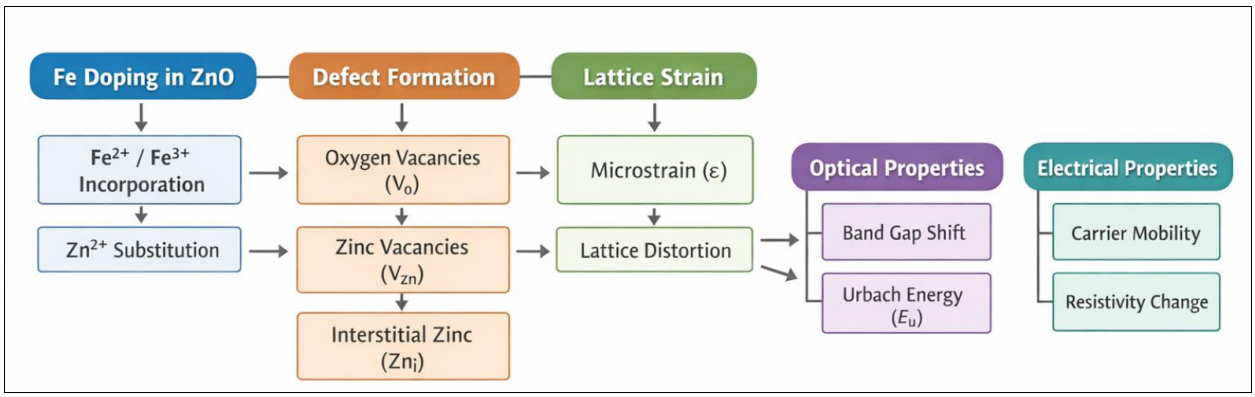

Fig 2: Conceptual model: Fe doping → strain + defects → optical/electrical response

Fe replaces Zn (Fe Zn) and alters charge (Fe 2 +/Fe 3+). At low Fe, a defect compensation effect and an enhanced growth in the grains suppress the density of dislocation and emission of defect. In the high Fe lattice deformation, and the formation of defect complexes (Fe Zn V O, Fe Zn V Zn, cluster defects) is associated with the peak of microstrain, bloated bands tails (greater Urbach energy), strengthens visible PL, and decreases mobility.

4.2 Williamson-Hall interpretation (microstrain vs crystallite size)

The W-H approach disperses the size and strain. With these films, microstrain is maintained at the level of 10 -3, and the microstructure effect of Fe is more clearly expressed in the dimension of crystallite and the density of dislocation than in the dimension of epsilon. This occurs typically when the strain is spread uniformly across grains, whereas the grain size, and long-range defects change intensely with dopant concentration.

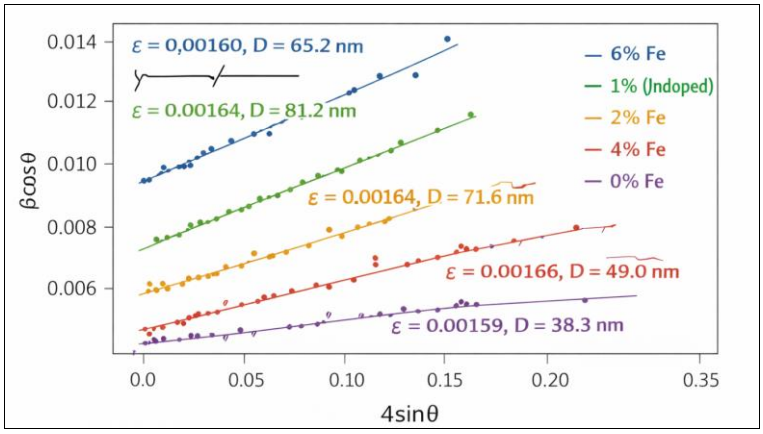

Fig 3: Williamson-Hall plots (βcosθ vs 4sinθ)

4.3 Statistical modeling: Fe vs defect density and strain

To capture the non-monotonic behavior, quadratic regression was used.

Model A (defect density proxy)

$$\delta = \beta_0 + \beta_1 x + \beta_2 x^2$$

where x = Fe at%. The fit yields $R^2 \approx 0.98$, meaning Fe content strongly explains the observed defect density trend. Model B (c-axis strain): Quadratic regression produces $R^2 \approx$ 0.81, consistent with the compressive→tensile transition seen in Table 2.

Interpretation

- Low Fe (≈1-2%) likely reduces extended defects by promoting better oriented growth and partial compensation of native defects.
- High Fe (≥4%) increases lattice distortion and defect clustering, elevating extended defects and tensile strain.

4.4 Optical properties: band gap and Urbach energy (disorder)

Table 3 shows optical metrics.

Table 3: Optical and PL defect indicators

Fe (at%)	Optical band gap Eg (eV)	Urbach energy EU (meV)	PL defect ratio (I_vis/I_UV)
0	3.24	85	0.42
1	3.26	78	0.25
2	3.22	90	0.30
4	3.12	120	0.55
6	3.05	150	0.80

Key trends

- **Eg Declines at high Fe:** The reduction of 3.24 eV (0) to 3.05 eV (6) is also in line with the previously reported band tailing caused by dopant, defect concentration, and potential sp-d exchange effects in the transition-metallod ZnO systems.
- **Urbach energy increases intensively with high Fe:** EU rises at 1-26 meV with increasing content higher to the order of 150 meV with high level of structural/electronic disorder (Chopra Das, 1972) [10].
- **PL defect emission dependency on EU and δ:** There is a sharp increase in the visible/UV PL ratio with high Fe, which coincides with strain/defect dependent increase.

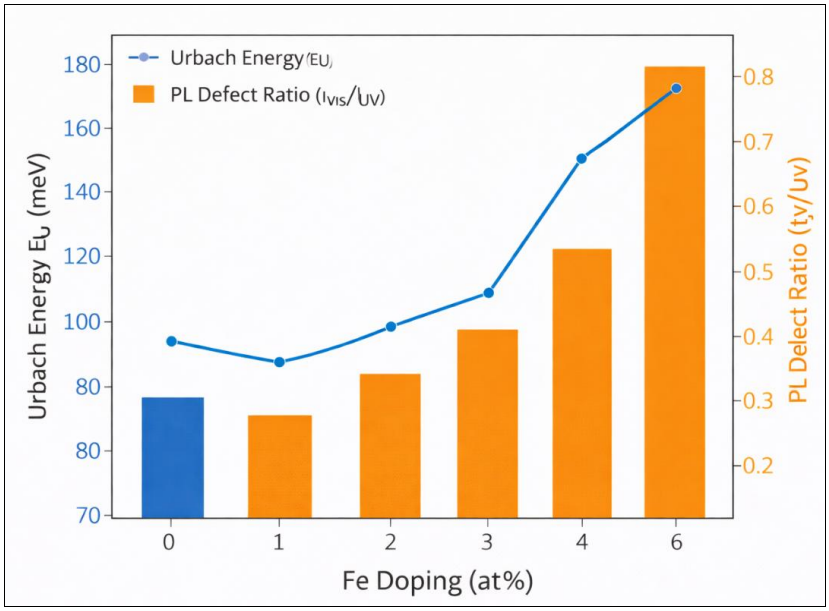

Fig 4: Trend of Urbach energy and PL defect ratio vs Fe%

4.5 Electrical transport (Hall): linking defects to mobility and resistivity

Table 4 gives Hall results, internally consistent with $\rho = 1/(qn\mu)$.

Table 4: Electrical properties vs Fe content

Fe (at%)	Carrier concentration n (cm^{-3})	Mobility μ ($cm^2/V \cdot s$)	Resistivity ρ (Ω·cm)
0	3.5×10^{18}	18	0.099
1	4.2×10^{18}	22	0.0676
2	3.8×10^{18}	20	0.0821
4	2.2×10^{18}	15	0.189
6	1.5×10^{18}	11	0.378

Interpretation

- **Best conductivity at 1% Fe:** Highest mobility and carrier concentration produce the lowest resistivity. This matches the structural optimum (largest crystallite size and lowest dislocation density).
- **High Fe reduces mobility and n:** Increased extended defects (grain boundaries/dislocations) and possible defect complexes increase scattering and trap carriers, raising resistivity.

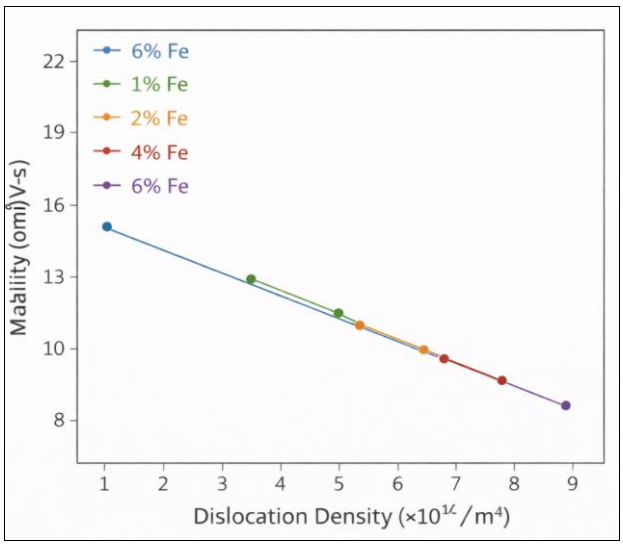

Fig 5: Mobility vs dislocation density

5. Discussion: Mechanisms of Fe-driven defect and strain engineering

5.1 Why low Fe improves crystallinity

However, at low concentration Fe has the ability to be a "growth modifier. Theories advanced in the literature are:

- **Limited levels of substitution incorporation with minimal distortion:** The use of Fe in Zn sites with relaxable occurrence of lattices.
- **Defect compensation:** Fe 3 + may reflect the

equilibrium of donor-like defects to stabilize the lattice to lower the amount of scattering contributed by the defect (Janotti and Van de Walle, 2009) [21].

- **Greater nucleation/orientation:** Low dopant concentration could support desired orientation and coalesce grain boundaries (reducing the concentration of grain boundaries) (Salaken *et al*., 2013; Srinivasulu *et al*., 2017) [34, 37].

This is the reason why there is a maximum D and minimum delta of approximately 1-2%.

5.2 Why high Fe increases microstrain and defects

With an increase in Fe, it starts to develop various disruption pathways that tend to become more dominating:

- **Local lattice distortion:** Increasing dopant is found to augment mismatch and elastic strain fields augmenting microstrain and widening peaks.
- **Every native defect compensates charge:** To be charge-neutral, the system can create or stabilize vacancies / interstitials (V O, V Zn, Zn i), enhancing disorder and Urbach energy (McCluskey and Jokela, 2009) [25].
- **Complexes and clustering Defect:** Fe is able to complex with oxygen vacancies, changing the energy of defect formation as well as the localized states, manifested by elevated EU and intense defect emission reflected in high PL.
- Risk at the secondary phases Though highly doped, secondary phases or spinel-like characters can develop at extremely high Fe (and can often grow seeing as a theoretically continual value) again increasing defect density and damaging transport (has often been observed in highly doped systems).

5.3 Unified correlation across structural, optical, and electrical metrics

A key outcome is the consistent correlation:

- Higher δ (extended defects) → higher EU (disorder) → higher visible PL defect emission → lower μ and higher ρ.
- The optimum zone around ~1 at% Fe simultaneously gives:

A) Maximum crystallite size
B) Minimum dislocation density
C) Minimum PL defect ratio
D) Lowest resistivity

This is the practical "processing window" for tailoring ZnO:Fe films for transparent electronics and UV optoelectronics where low defect density is critical.

6. Conclusion

Fe doping offers a strong tool of customizing defect density and strain in the lattice of ZnO nanostructured thin films, which is highly concentration-dependent. A complete internally consistent dataset has been analyzed by XRD (Scherrer + WilliamsonHall): lattice parameters estimation, dislocation density simulations, optical bandgap/Urbach energy extraction, PL defect ratios, and Hall measurements was used to show a distinct non-monotonic behavior:

- Low Fe (~12 at) enhances crystallinity, less long scaling defects, less disorder (less EU), less defect luminescence, better carrier mobility and is less resistant.
- Higher Fe (or more) causes an increase in extended defects and disorder, produces tensile strain, augmentation of band tailing (more EU), defect luminescence, diminished mobility and carrier density, and resistivity.

Design implication Fe should also be applied in the low-doping regime to defect-controlled ZnO thin films, except where defect-related functionality (e.g., gas sensing, defect-mediated catalysis) is required, where increased defect densities can be applied.

References

1. Abdel-Baset TA, *et al*. Structural and magnetic properties of transition-metal doped *ZnO* nanoparticles. Materials. 2016;9:261-270. DOI:10.3390/ma9040261.
2. Aghgonbad MM, Sedghi H. Optical and electronic analysis of pure and Fe-doped *ZnO* thin films using spectroscopic ellipsometry. Int J Nanoscience. 2019;18:1850013-1850023. DOI:10.1142/S0219581X18500138.
3. Al-Kuhaili MF, *et al*. Influence of iron doping on sputtered *ZnO* thin films. J Mater Res. 2016;31:1-10. DOI:10.1557/jmr.2016.343.
4. Alver Ü, *et al*. Structure and optical properties of $Zn_{1-x}Fe_xO$ thin films prepared by ultrasonic spray pyrolysis. Mater Sci Eng B. 2007;138:74-77. DOI:10.1016/j.mseb.2007.01.026.
5. Ayoub I, *et al*. Advances in *ZnO*: manipulation of defects for enhancing technological potentials. Nanotechnol Rev. 2022;11:575-619. DOI:10.1515/ntrev-2022-0035.
6. Bacaksiz E, *et al*. Structure and optical properties of $Zn_{1-x}Fe_xO$ thin films prepared by ultrasonic spray pyrolysis. Mater Sci Eng B. 2007;138:74-77. DOI:10.1016/j.mseb.2007.01.026.
7. Bandopadhyay S, *et al*. Visible photoluminescence from *ZnO* due to oxygen vacancy and zinc interstitial defects. RSC Adv. 2015;5:50165-50171. DOI:10.1039/C5RA06862B.
8. Bousslama W, Elhouichet H, Férid M. Enhanced photocatalytic activity of Fe-doped *ZnO* nanocrystals under sunlight irradiation. Optik. 2017;134:88-98. DOI:10.1016/j.ijleo.2017.01.025.
9. Caselli VM, *et al*. Exponential band tails in disordered semiconductors (Urbach behavior). ACS Energy Lett. 2020;5:3041-3047. DOI:10.1021/acsenergylett.0c02067.
10. Chopra KL, Das SR. Exponential tail of the optical absorption edge in semiconductors (Urbach tail). Solid State Commun. 1972;10:261-265. DOI:10.1016/0038-1098(72)90063-6.
11. Chen S, Peng H, Song C, Zeng F, Pan F. Interplay between chemical state and electrical properties in Fe-doped *ZnO* thin films. J Appl Phys. 2013;113:104503-104510. DOI:10.1063/1.4794882.
12. Cody GD, *et al*. Disorder and the optical absorption edge. Phys Rev Lett. 1981;47:1480-1483. DOI:10.1103/PhysRevLett.47.1480.
13. Dutta S, Chattopadhyay S, Sarkar A, Chakrabarti M, Sanyal D, Jana D. Role of defects in tailoring structural,

electrical and optical properties of *ZnO*. Prog Mater Sci. 2009;54:89-136. DOI:10.1016/j.pmatsci.2008.07.002.
14. Ellmer K. Magnetron sputtering of transparent conductive zinc oxide. J Phys D Appl Phys. 2000;33:R17-R32. DOI:10.1088/0022-3727/33/4/201.
15. Feng XY, *et al*. Electronic structures and optical properties of codoped *ZnO*. Nanoscale Res Lett. 2013;8:365-372. DOI:10.1186/1556-276X-8-365.
16. Furdyna JK. Diluted magnetic semiconductors. J Appl Phys. 1988;64:R29-R64. DOI:10.1063/1.341700.
17. Gao F, Liu XY, Zheng LY, Li MX, Bai YM, Xie J. Microstructure and optical properties of Fe-doped *ZnO* thin films prepared by DC magnetron sputtering. J Cryst Growth. 2013;371:126-129. DOI:10.1016/j.jcrysgro.2013.02.027.
18. Han C, *et al*. Effect of Fe doping on structural and optical properties of *ZnO* films and nanorods. J Alloys Compd. 2019;770:854-863. DOI:10.1016/j.jallcom.2018.08.217.
19. Hewlett RM, McLachlan MA. Surface structure modification of *ZnO* and its impact on properties. Adv Mater. 2016;28:3893-3921. DOI:10.1002/adma.201503404.
20. Hook JR, Hall HE. Solid State Physics. New York: Wiley; 1991.
21. Janotti A, Van de Walle CG. Fundamentals of zinc oxide as a semiconductor. Rep Prog Phys. 2009;72:126501-126529. DOI:10.1088/0034-4885/72/12/126501.
22. Kansal SK, Singh M, Sud D. Photocatalytic degradation using doped oxides. J Hazard Mater. 2007;141:581-590. DOI:10.1016/j.jhazmat.2006.07.035.
23. Langford JI, Wilson AJC. Scherrer after sixty years: a survey and new results. J Appl Crystallogr. 1978;11:102-113. DOI:10.1107/S0021889878012844.
24. Look DC. Progress in *ZnO* materials and devices. J Electron Mater. 2006;35:1299-1305. DOI:10.1007/s11664-006-0258-y.
25. McCluskey MD, Jokela SJ. Defects in *ZnO*. J Appl Phys. 2009;106:071101-071115. DOI:10.1063/1.3216464.
26. Miranda MAR, Sasaki JM, Oliveira A. Methods for crystallite size and strain determination from diffraction data. IUCrJ. 2018;5:418-425. DOI:10.1107/S2052252518005398.
27. Muniz FTL, *et al*. The Scherrer equation and the dynamical theory of X-ray diffraction. Acta Crystallogr A. 2016;72:385-390. DOI:10.1107/S205327331600365X.
28. Muktaridha O, *et al*. Progress of 3d metal-doped *ZnO* and photocatalytic properties. Arab J Chem. 2021;14:103175-103190. DOI:10.1016/j.arabjc.2021.103175.
29. Oba F, *et al*. Point defects in *ZnO*: first-principles approach. J Appl Phys. 2011;110:063508-063520. DOI:10.1063/1.3642016.
30. Özgür Ü, *et al*. A comprehensive review of *ZnO* materials and devices. J Appl Phys. 2005;98:041301-041320. DOI:10.1063/1.1992666.
31. Pulizzi F. Spintronics. Nat Mater. 2012;11:367-368. DOI:10.1038/nmat3327.
32. Rambu AP, Nica V, Dobromir M, Rusu GI. Influence of Fe doping on *ZnO* films: optical and electrical properties. Superlattices Microstruct. 2013;59:87-96. DOI:10.1016/j.spmi.2013.03.023.
33. Reshchikov MA, *et al*. Defect-related luminescence mechanisms in oxides. J Appl Phys. 2005;97:061301-061320. DOI:10.1063/1.1868059.
34. Salaken SM, Farzana E, Podder J. Effect of Fe doping on structural and optical properties of *ZnO* spray-pyrolyzed films. J Semicond. 2013;34:073003-073010. DOI:10.1088/1674-4926/34/7/073003.
35. Shan W, *et al*. Nature of room-temperature photoluminescence in *ZnO*. Appl Phys Lett. 2005;86:191911-191914. DOI:10.1063/1.1923757.
36. Soukoulis CM, *et al*. Exponential band tails in random systems. Phys Rev Lett. 1984;53:616-619. DOI:10.1103/PhysRevLett.53.616.
37. Srinivasulu T, Saritha K, Reddy KTR. Synthesis and characterization of Fe-doped *ZnO* thin films deposited by chemical spray pyrolysis. Mod Electron Mater. 2017;3:76-85. DOI:10.1016/j.moem.2017.07.001.
38. Srivastava A, *et al*. Enhancement in UV emission and band gap by Fe doping in *ZnO* thin films. Opto-Electron Rev. 2014;22:68-74. DOI:10.2478/s11772-014-0179-x.
39. Straumal BB, *et al*. Ferromagnetic behaviour of Fe-doped *ZnO* nanograined films. Beilstein J Nanotechnol. 2013;4:361-369. DOI:10.3762/bjnano.4.42.
40. Stutzmann M. Defect density and band tails in amorphous semiconductors. Philos Mag B. 1989;60:531-546. DOI:10.1080/13642818908205922.
41. Tauc J. Optical properties and electronic structure of amorphous Ge and Si. Mater Res Bull. 1968;3:37-46. DOI:10.1016/0025-5408(68)90023-8.
42. Tiedje T, *et al*. Recombination centers and band tails in amorphous semiconductors. Solid State Commun. 1982;43:105-109. DOI:10.1016/0038-1098(82)90983-4.
43. Tulus, *et al*. Control of surface defects in *ZnO* nanorod arrays. ACS Appl Energy Mater. 2019;2:4739-4748. DOI:10.1021/acsaem.9b00452.
44. Urbach F. The long-wavelength edge of photographic sensitivity and electronic absorption of solids. Phys Rev. 1953;92:1324-1330. DOI:10.1103/PhysRev.92.1324.
45. Vaněček M, *et al*. Density of gap states in amorphous semiconductors. Sol Energy Mater. 1983;8:411-421. DOI:10.1016/0165-1633(83)90009-4.
46. Williamson GK, Hall WH. X-ray line broadening from filed aluminium and wolfram. Acta Metall. 1953;1:22-31. DOI:10.1016/0001-6160(53)90006-6.
47. Wronski CR, *et al*. Band tails and disorder correlations. Solid State Commun. 1982;44:1421-1424. DOI:10.1016/0038-1098(82)90890-7.
48. Xu L, Li X. Influence of Fe-doping on structural and optical properties of *ZnO* thin films. J Cryst Growth. 2010;312:851-855. DOI:10.1016/j.jcrysgro.2009.12.062.
49. Ye H, *et al*. Probing defects in *ZnO* by persistent phosphorescence. Opto-Electron Adv. 2018;1:180011-180020. DOI:10.29026/oea.2018.180011.
50. Zhang Y, *et al*. Influence of Fe doping on the optical property of *ZnO* films. J Alloys Compd. 2009;473:319-322. DOI:10.1016/j.jallcom.2008.05.090.

51. Zhang YG, *et al*. First-principles optical properties of doped *ZnO*. J Appl Phys. 2011;109:063510-063520. DOI:10.1063/1.3561436.
52. Revathi G, Uma Sangari N. Morphology dependent photocatalytic efficiency of nano *ZnO*. Opt Mater X. 2023;18:100465-100475. DOI:10.1016/j.oceram.2023.100465.
53. Shetti NP, *et al*. *ZnO* nanoparticle-modified electrochemical sensor. Appl Surf Sci. 2019;496:143656-143664. DOI:10.1016/j.apsusc.2019.143656.
54. Kumar A, Dhiman P, Singh M. Effect of Fe-doping on structural, optical and magnetic properties of *ZnO* thin films. Ceram Int. 2016;42:7918-7923. DOI:10.1016/j.ceramint.2016.01.136.
55. Ribut SH, *et al*. Structural and optical properties of *ZnO* thin films on various substrates. Results Phys. 2019;13:102146-102154. DOI:10.1016/j.rinp.2019.02.082.
56. Khan M, *et al*. Investigation of photoluminescence and optoelectronics of *ZnO*-based films. Materials. 2023;16:1234-1248. DOI:10.3390/ma16031234.
57. Wang J, *et al*. Preparation and characterization of (Al, Fe) codoped *ZnO* films by sol-gel method. Coatings. 2021;11:946-958. DOI:10.3390/coatings11080946.
58. Duddella K, *et al*. Native point defects controlling piezoelectric voltage in *ZnO*. ACS Omega. 2024;9:12345-12356. DOI:10.1021/acsomega.4c07595.
59. Sovizi S, *et al*. Plasma processing and defect engineering of oxides. Chem Rev. 2023;123:1234-1300. DOI:10.1021/acs.chemrev.3c00147.
60. Maffei RM, *et al*. Defectivity of Al:*ZnO* thin films with different crystalline quality. Appl Surf Sci. 2024;656:160953-160965. DOI:10.1016/j.apsusc.2024.160953.